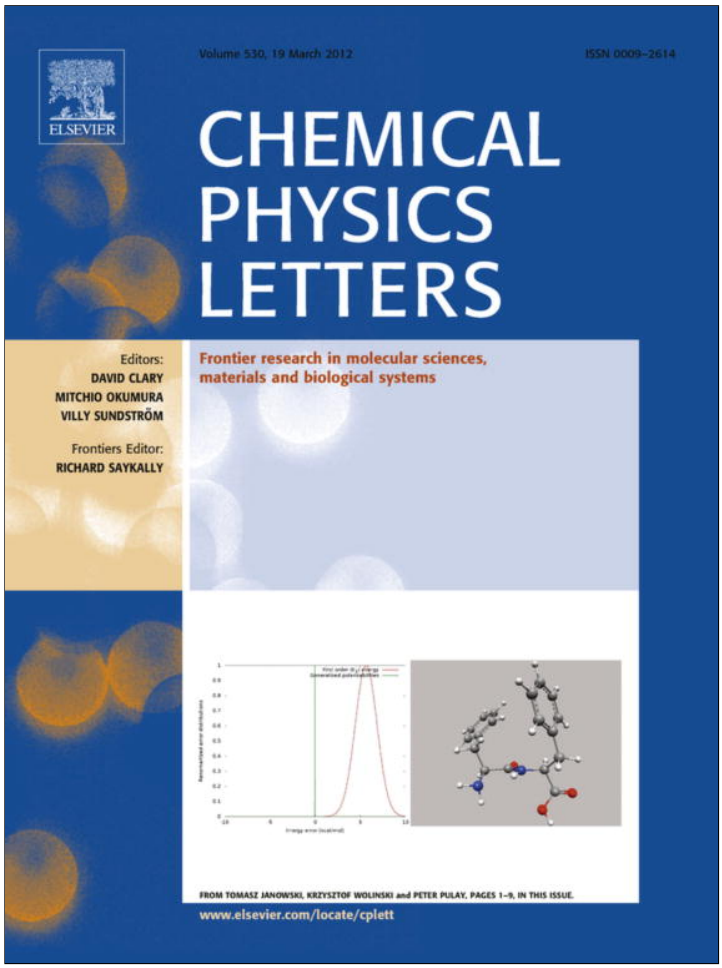

Chemical Physics Letters 530 (2012) 93–97

Contents lists available at SciVerse ScienceDirect

Chemical Physics Letters

journal homepage: www.elsevier.com/locate/cplett

Fabrication and characterization of aluminum nanostructures and nanoparticles obtained using femtosecond ablation technique

G. Krishna Podagatlapalli [a], Syed Hamad [b], S. Sreedhar [a], Surya P. Tewari [a,b], S. Venugopal Rao [a,*]

[a] Advanced Center of Research in Higher Energy Materials (ACRHEM), University of Hyderabad, Hyderabad 500046, India
[b] School of Physics, University of Hyderabad, Hyderabad 500046, India

ARTICLE INFO

Article history:
Received 14 November 2011
In final form 31 January 2012
Available online 8 February 2012

ABSTRACT

In this communication we report the fabrication of nanoparticles (NPs) and nanostructures through the interaction of ultrashort laser pulses (~40 fs) with bulk aluminum immersed in chloroform and carbon tetrachloride. The size distribution and surface morphology of substrates were investigated using scanning electron microscope images. Depending on the focal position we observed sub-micron structures and nano-ripples on the irradiated surface. Picosecond nonlinear optical studies of the prepared NPs colloidal solutions using open aperture Z-scan technique demonstrated complex behavior of switching from saturable absorption to reverse saturable absorption (RSA) at lower peak intensities to pure RSA at higher peak intensities.

1. Introduction

Nanoparticles synthesis and their characterizations are of great interest in present day advancement of science because of the physics associated with them and are described by the intermediate regime between quantum physics and classical physics [1]. The electronic properties of nano-sized systems change dramatically since the density of states and spatial length scale of electronic motion are reduced with decreasing size. For these nano-entities, Eigen states are determined by the systems boundaries and hence the surface effects become very important [2]. NPs can be produced by variety of methods such as arc discharge [3], vapor deposition [4], electrochemical deposition [5], or ball milling [6] and laser ablation using nanosecond (ns) or femtosecond (fs) pulses. Femtosecond laser ablation (FLA) is one of the best methods to generate impurity free nanoparticles of narrower size distribution and with reduced porosity [7]. Laser ablation of metals immersed in liquid medium has advantages that it can generate well dispersed and less oxidized NPs (with necessary precautions). Furthermore, as generated nanoparticles remain in the liquid in which ablation takes place, it can reduce the contamination of the surrounding air medium from the expulsion of generated nanoparticles into it. This technique provides the possibility of generating a large variety of NPs those are free of both surface-active substances and counter ions [8,9]. If the input laser energy density is high enough than the damage threshold of metal used, then the deposition of high energy density through a fs laser pulse on a metal immersed in liquid results in rapid heating of the surface to high temperatures (due to large peak intensities) eventually leading to plasma formation [10]. As a result, surface of the target melts and the melt is subsequently dispersed in the surrounding liquid and formation of nanostructures take place on substrate because of the recoil pressure of the liquid vapor surrounding the laser beam waist at the focus on the surface of target. Rapid expansion and cooling of solid matter result in NP synthesis. In this process along with nanoparticles, free atoms, ions and target fragments emanate from the plume. When a metal passes through a melt state due to ablation, stimulation of the physicochemical processes of interaction of metal with liquid medium takes place causing the formation of complex structures instead of usual spherical particles. Such colloidal solutions have optical and nonlinear optical characteristics that are different from colloids prepared by other methods [11]. The growth of nanoparticles and aggregation takes place under the influence of surrounding liquid environment and aggregation depends upon the permittivity and the polarity of the surrounding liquid medium [12]. Upon ablation of solids within liquid environment the molten layer borders directly on the vapor of ambient liquid. Under these conditions the viscous interaction of vapor on the target surface with molten target layer may be responsible for several instabilities like Kelvin–Helmholtz or Rayleigh–Taylor instabilities. These instabilities are tentatively assigned to the observed nanostructure formation on the substrate [13]. Femtosecond laser pulses allow the completion of energy deposition into the target well before the target expansion begins thereby reducing unwanted interaction of laser pulse with the generated plasma. FLA can be considered as isochoric process (considerable change of volume of sample does not occur) since the irradiation of laser pulse causes local heating in short

* Corresponding author. Fax: +91 040 23012800.
E-mail addresses: soma_venu@yahoo.com, svrsp@uohyd.ernet.in (S. Venugopal Rao).

0009-2614/$ - see front matter © 2012 Elsevier B.V. All rights reserved.
doi:10.1016/j.cplett.2012.01.081

time and it lasts before expansion of metal takes place. The main advantage of the ablation of metals in liquid media in comparison with other chemical methods is lesser need to add surfactant for capping of NPs.

Al is the cheapest metal among the plasmonic metals such as Au, Ag, and it has low melting point (660 °C), hence Al nanoparticles can be easily generated. As surface area to volume ratio is high, these are used as fuels in high energetic material applications like propellants, munitions, and pyrotechnics and can be used as additives for plastics and powder metallurgy [14]. Al NPs particles provide enhanced heat release during their exothermal oxidation. The rate of reactivity increases as the size of Al NP decreases (bare Al is highly reactive). Since Al is highly reactive to ambient oxygen, fabrication of pure Al NPs is restricted by the oxidation effects which reduce the reactivity, burn rate, and hence the velocity of detonation. This effect becomes more pronounced as particle size decreases, since the oxide layer represents a significant fraction of its mass [13]. In this context, fs laser pulses are helpful in quenching of nanostructured Al and thus preserve its metallic nature as it is due to the shorter time of interaction with liquid environment. We have taken the liquid media which are free from oxygen to reduce the effect of oxidation since one of the barriers for bare Al NPs formation is the dissolved oxygen in liquid medium in which ablation takes place. In this Letter, we report nanoparticle fabrication from bulk Al in liquids such as carbon tetrachloride and chloroform, Al nanostructure formation on the substrate in the laser exposed region, and the nonlinear optical studies of Al NPs colloidal solutions.

2. Experiment

Pure Al targets were washed with acetone after sonication to remove organic dopants from the surface. The source was a chirped pulse amplified (CPA) of Ti:sapphire laser system (LEGEND, Coherent) delivering nearly bandwidth limited laser pulses (~40 fs, 1 kHz repetition rate) at 800 nm as an excitation source. The amplifier was seeded with ~15 fs (55-60 nm FWHM) pulses from an oscillator (MICRA, Coherent, 1 W, 80 MHz, 800 nm). The average and peak powers after the amplifier were 2.5 W and 67 GW, respectively. The target was placed into a Pyrex cell and covered by a layer of absolute liquids – CCl_4 and $CHCl_3$. After ensuring the sample was perfectly parallel to the optical bench, laser pulses (S polarized) were allowed to focus onto the Al sample using a plano-convex lens of focal length 8 cm. Typical pulse energies used were ~250 μJ. The position of the focus was approximated to lie at the point where plasma was generated. It is important to adjust the focus exactly on the surface of substrate immersed in liquid taking into account the refractive index of liquid. We could manually change the position of the focus beyond the sample and exactly on the surface of the sample using a translational stage (along Z-direction) on which the sample was fixed. We noticed that for achieving better rate of nanoparticles formation the focus should be on the surface of substrate. The beam waist estimated at the focus was ~15 μm. The level of liquid was ~2-3 mm above the Al sample. The Al targets were placed normal to the laser beam on a motorized X–Y stage, operated through the motion controller (Newport ESP 300). The scanning speeds of the X–Y stages were 0.2 and 0.4 mm/sec. The motorized stages were moved in such a way to write periodic lines on the Al sample (separation of ~150 μm). Time of exposure was ~5 min. We observed that the liquid in which the ablation was carried out turned to gold–yellow color due to the dispersion of ejected Al nanoparticles into liquid [15]. The coloration of the NPs colloidal solution of Chloroform was thicker (dark yellow) than CCl_4 colloidal solution. FESEM (Ultra 55 from Carl ZEISS) analysis and the UV absorption spectra and Energy Dispersive Spectrometer (OX-Ford Instruments) of the colloidal solutions proved the presence of well dispersed nanoparticles. EDX spectra were used to identify the constituents of the nanoparticles. We observed that the coloration of the laser exposed portion on the metal changed to yellow color. Simultaneously, we observed nanostructure formation on the substrate as previously reported mushroom structures by Stratakis et al. [15,16]. The nonlinear optical properties of the NPs colloidal solutions were investigated using open aperture Z-scan method [17,18] with 1 kHz, 800 nm laser pulses (~2 mJ, ~2 ps duration). Complete details of the setup are reported in our earlier works [19,20,31]. The colloidal solution was taken in a Quartz cuvette of 1 mm path length. Z-scan studies were performed by focusing the 4 mm diameter input beam using a lens (f = 20 cm). The beam waist at the focus was ~25 μm.

3. Results and discussion

During the ablation in chloroform, colloidal solution became opaque initially and turned to pale yellowish finally (exposure time of 5 min). CCl_4 medium became opaque faster than chloroform and its color also turned to gray–yellow. Visible comparison of synthesized colloidal samples demonstrated that the sample CCl_4 was dark in color than chloroform. FESEM images of a drop of CCl_4 (Figure 1a) and $CHCl_3$ (Figure 1c) NPs colloidal solutions taken on a carbon tape emphasized that well dispersed Al nanoparticles of different sizes ranging from 5 to 40 nm were generated. From the nanoparticle distribution histogram we could observe the average size distribution in CCl_4 [top in the inset of Figure 1a) to be 30 and 15 nm in $CHCl_3$ (top in the inset of Figure 1c). The reason for narrow distribution of nanoparticles in chloroform was the polarity of its molecules. As chloroform is a polar solvent its molecules strongly attracts the charged surface of Al NPs and thus form electrical double layers (EDL) on NPs surface, which in turn ceases the further growth of nanoparticles as it screens the surface of nanoparticles from surrounding environment, finally resulting in less particle growth and hence narrow distribution [12]. CCl_4 is a non-polar solvent (zero polarity of the molecules) and therefore it could not prevent the further growth of nanoparticles formed. The growth took place until free atoms and ions present in the colloidal solution. Because of this reason distribution of Al NPs in CCl_4 was slightly broader. EDS spectrum was taken for the both colloidal (CCl_4 & $CHCl_3$) drops. Bottom figures in the inset of Figure 1a and c shows the EDX spectrum which confirms the metallic nature of fabricated Al nanoparticles in colloidal CCl_4 and $CHCl_3$, respectively. From the EDS we could conclude that the metallic nature of the Al was prevailed than oxygen content in the generated nanoparticles. TEM images confirmed the presence of a thin layer, of possibly Al_2O_3, on Al NPs. Since we performed the ablation in liquid environment, which was free from oxygen, instantaneous oxidation taking place at the time of condensation of metal melt reduced to some extent. We observed that rate of particle formation depends upon many factors such as exposure time, liquid level, and laser beam parameters (fluence, beam waist, wavelength).

We did not observe any color change in colloidal solution even after 4 weeks indicating their stability. UV–Vis absorption spectra of colloidal solutions are presented in Figure 1b (CCl_4) and 1d (chloroform). Al NPs solutions synthesized in ethanol and acetone demonstrated absorption peak near 210 nm proving the presence of Al NPs and not alumina [15,16]. Baladi et al. [21] reported that Al nanoparticle colloids show a characteristic peak near 300 nm. UV-absorption peak of the colloidal solutions of CCl_4 (Figure 1b) was near 300 nm (weak). $CHCl_3$ solution (Figure 1d) exhibited one peak near 235 nm and a second weak absorption peak at 270 nm. These absorption peaks are the SPR (Surface Plasmon

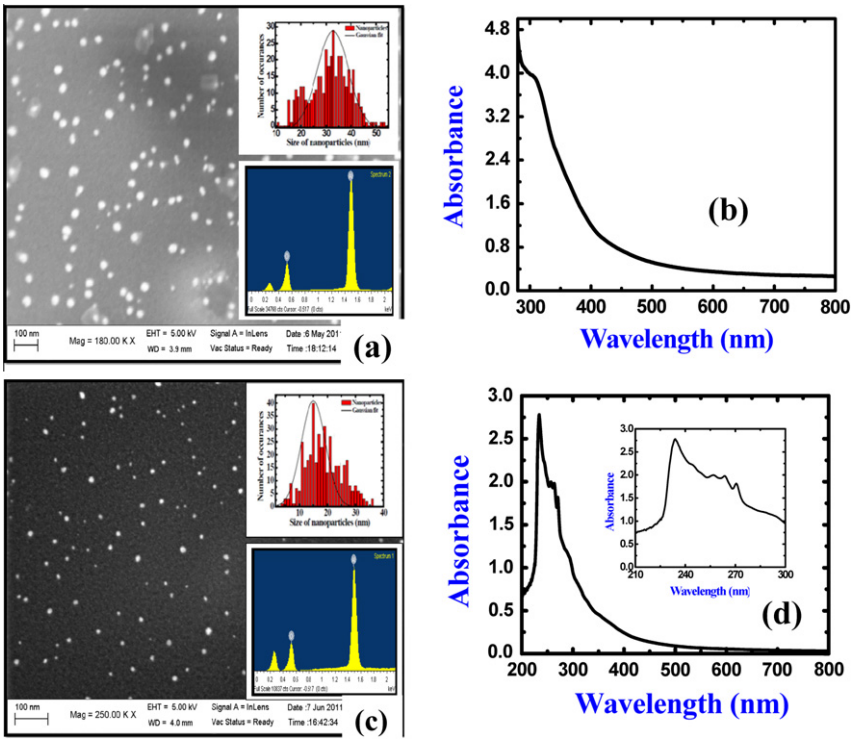

Figure 1. (a) FESEM image of CCl_4 colloidal solutions and inset shows their nanoparticle distributions (above) and EDX spectra (below) of the colloidal CCl_4, (b) UV–Vis extinction spectra of colloidal CCl_4 showing SPR peak in the neighborhood of 300 nm, (c) FESEM image of $CHCl_3$ colloidal solutions and inset shows their nanoparticle distributions (above) and EDX spectra of the colloidal $CHCl_3$ and (d) UV–Vis extinction spectra of colloidal $CHCl_3$ showing SPR peak in the neighborhood of 235 nm (pure Al) and small SPR peak at 270 nm. S-polarization was used for all the data presented here.

Resonances) peaks. The remaining peaks in spectrum (inset of Figure 1d) could be from bond dissociations of the surrounding liquid molecules. The SPR peak position depends on the dielectric function of surrounding medium. The red shift in SPR peak (for $CHCl_3$) may be explained on the basis of nanoparticle size. The larger the particles become the importance of higher order modes increases since the light can no longer polarize the nanoparticles homogeneously. These higher order modes peak at lower energies and therefore the Plasmon peak position shifts with increasing particle size. Therefore, we could conclude that the average size of fabricated Al nanoparticles in CCl_4 (non-polar) was greater than in $CHCl_3$ (polar). This was also confirmed through FESEM images. Laser exposed region of Al target acquired yellowish color being visible at angles close to normal incidence. The coloration of the Al strip was more pronounced when ablation was carried out in water at a fluence of ~2–3 J/cm^2. This coloration can be assigned to structuring of Al surface and similar nanostructures were previously reported on both Ag and Au [22,23].

There was no change in coloration of water after ablation, which was confirmed from SEM images where we observed aggregation. Depending on the focusing conditions, we observed different patterns on the Al substrate. Figure 2a shows the FESEM image of the laser exposed Al substrate in water, exhibiting a micro grating formation with nearly periodic craters. This structure was observed only when the focus of the laser beam was on the sample surface (higher fluence). Figure 2b shows the FESEM image of nano-ripples (with a period ~330 nm) which were observed on the Al substrate immersed in water, when the focus was beyond the surface of the Al substrate (lower fluence). The interference of incident electromagnetic wave with surface electromagnetic wave generated on the substrate could be the reason for observing these nanostructures. A closer view of these ripples demonstrated mushroom like nanostructures (Figure 2c), tentatively assigned to Rayleigh–Taylor like instabilities. Under the above mentioned instabilities redistribution of the melt takes place and results in mushroom like structures [13]. For the above mentioned fluence and scanning speeds, we repeated the ablation in CCl_4 and $CHCl_3$ but we did not observe any coloration on the Al substrate where as the liquids became yellowish. At lower fluence (<0.05 J/cm^2), virtually no changes of the Al surface [14] and liquid were observed, even with elevated number of laser shots. FESEM images of the laser exposed portions of Al substrate in CCl_4 (Figure 2d and e with 2f depicting closer view) and $CHCl_3$ (Figure 2g and h with 2i depicting closer views) demonstrated microstructure formation and mushroom like structures. Similar structures were obtained for P-polarized and circularly polarized pulses. Our ultimate aim is to produce nanostructured Al substrate to achieve enhanced Raman signal (SERS) [24] for explosives detection. Creating patterned surface structures with fs pulses yields high electric fields when used in conjunction with methods such as lithography or laser machining (e.g. in silver nitrate solutions or on Ag-doped materials).

Figure 3a shows the open aperture data of Al NPs colloidal solution of CCl_4 recorded at 800 nm and with three peak intensities of 96 GW/cm^2 (open circles), 130 GW/cm^2 (open triangles), and 190 GW/cm^2 (open squares). The optical properties of nano-sized metal particles can be described in terms of electron transitions between the discrete energy states in a quantum well subjected to the enhanced local field. Large enhancements of the local field inside a particle can be realized at the Plasmon resonance frequency. At lower peak intensities the behavior was switching and at higher intensities the behavior modified to pure reverse saturable absorption (RSA) with strong two photon absorption. The estimated magnitudes of two photon absorption (2PA) coefficients, saturation intensities, Im $[\chi^{(3)}]$ were 1.9×10^{-10} cm/W, 6.5 GW/cm^2, 6.4×10^{-12} e.s.u. (for peak intensity of 96 GW/cm^2), 3.3×10^{-10} cm/W, 5 GW/cm^2, 1.1×10^{-11} e.s.u. (for peak intensity of 130 GW/cm^2). For a peak intensity of 190 GW/cm^2 we observed 2PA (2×10^{-9} cm/W) corresponding to an Im $[\chi^{(3)}]$ of 6.7×10^{-11}

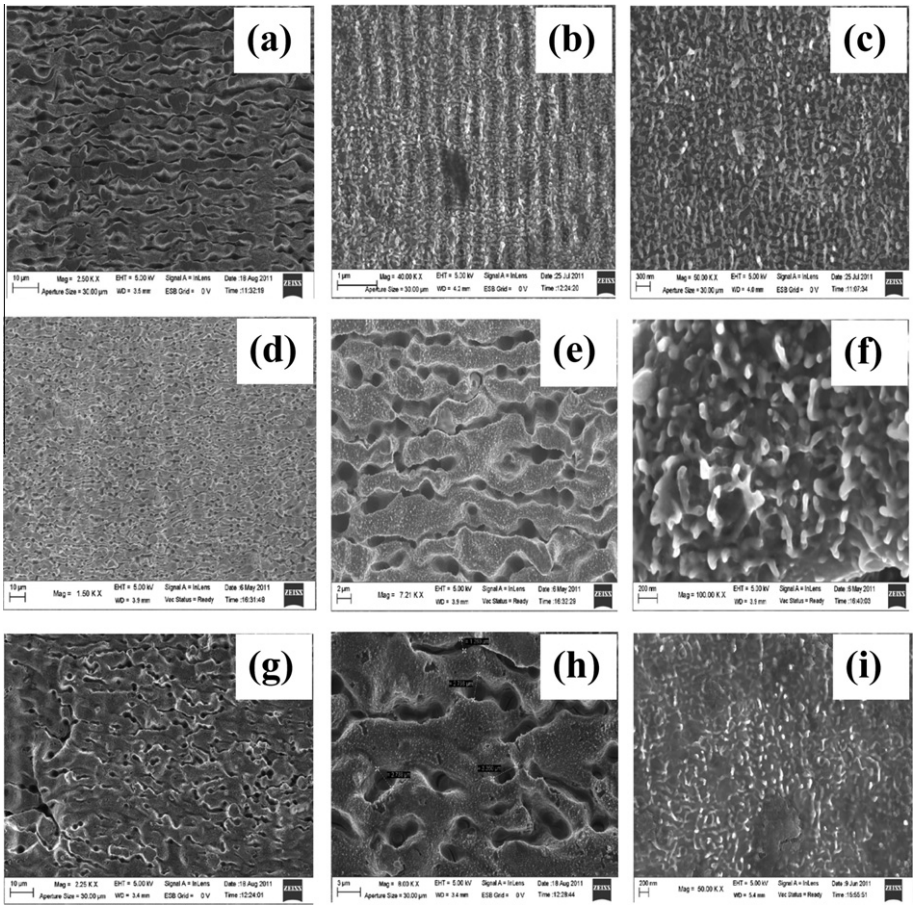

Figure 2. FESEM images of the laser exposed portion in the Al substrate in (a–c) water (a) micro-gratings were observed when the focus was on the substrate in solvent, (b) shows the image of the periodic nano-ripples observed on the Al substrate immersed in water. These ripples were observed when focus was beyond the surface of substrate and (c) magnified image of (b). (d)–(f) CCl_4, shows micro-gratings were observed when the focus was beyond the substrate in the range of (d) 10 μm scale, (e) 2 μm scale (magnified image), and (f) 200 nm scale, showing the mushroom like structure. (g)–(i) $CHCl_3$ showing the micro-gratings were observed when the focus was on the substrate in the range of (d) 10 μm scale, (e) 2 μm scale (magnified image), and (f) 200 nm scale, showing the mushroom like structure. S-polarization was used for all the data presented here.

e.s.u. Pure CCl_4 did not show any nonlinear absorption but the presence of nanoparticles (40% linear transmittance) introduced nonlinear absorption. Figure 3b shows the open aperture data of colloidal $CHCl_3$ (65% linear transmittance) recorded with same experimental conditions as mentioned above with peak intensities of 69 GW/cm^2 (open circles), 110 GW/cm^2 (open triangles), 140 GW/cm^2 (open squares), respectively. At lower peak intensities the behavior was switching and at higher intensities the behavior modified to reverse saturable absorption (pure RSA) with strong two photon absorption and their respective two photon absorption coefficients, saturation intensities, Im $[\chi^{(3)}]$ were 4.9×10^{-11} cm/W, 6 GW/cm^2, 1.6×10^{-12} e.s.u. (for peak intensity of 69 GW/cm^2). For peak intensities of 110 and 140 GW/cm^2 we observed 2PA (5×10^{-11} and 6.3×10^{-11} cm/W) with corresponding Im $[\chi^{(3)}]$ values of 1.7×10^{-12} e.s.u. and 2.1×10^{-12} e.s.u., respectively. To interpret and fit the data for the flip of saturable absorption near the beam waist, we combined saturable absorption coefficient and two photon absorption (TPA, β) coefficients yielding the total absorption coefficient [25–29]. We concluded that the observed nonlinear absorption was due to the metallic Al since the near IR light can be absorbed by Al but not by dielectric Al_2O_3 [30]. The nonlinear optical properties exhibited by the Al NPs colloidal solutions could be assigned to the generated excited states of the collective mode motion of conduction electrons in the Al nanoparticles (surface Plasmons). Probably the hot spots formed between the nanoparticles may be the reason for observed nonlinearities. Further studies are in progress to identify the correlation between nonlinearities and the size of NPs.

Rao et al. [31] studied the NLO properties of gold nanoparticles obtained using biosynthesis methods. Lee et al. [32] reported femtosecond NLO properties of gold nanocubes (65 nm) and nanooctahedra (49 nm) and observed SA with ~60 fs pulses (800 nm) at lower peak intensities (10–12 GW/cm^2) with magnitudes of 0.16 and 0.244 cm/GW while at higher peak intensities they observed 2PA with a magnitude of 2.5×10^{-10} cm/W. I_s calculated from their data was ~25 GW/cm^2. SA observed in their case was due to the bleaching of the ground state plasmon band. In the present study, though, the values of I_s are <10 GW/cm^2. Boni et al. [33] observed SA type of nonlinear absorption and achieved a β value of 0.1–0.7 cm/GW for gold nanospheres (~16 nm) at different wavelengths (500–600 nm), some of which were close to resonance. Reji et al. [34] studied gold nanoparticles (~3 nm) with 35 ps pulses (532 nm) and observed that ground-state plasmon bleach led to SA. Elim et al. [35] observed SA in gold nanorods (aspect ratio of 3.8) with ~220 fs pulses and obtained β to be ~1.5 cm/GW. However, there was a second absorption peak at 800 nm for their elongated structures making that a resonant excitation study. Sathyavathi et al. [36] studied the NLO properties of Ag NPs (average size of 26 nm) and obtained the values of n_2, β_{eff}, and $|\chi^{(3)}|$ to be -6×10^{-13} cm^2/W, 72.5 cm/GW, and 1.38×10^{-9} e.s.u., respectively. However, their studies were performed with a ns laser. Al is economic compared to Ag and Au and with FLA we can tailor the

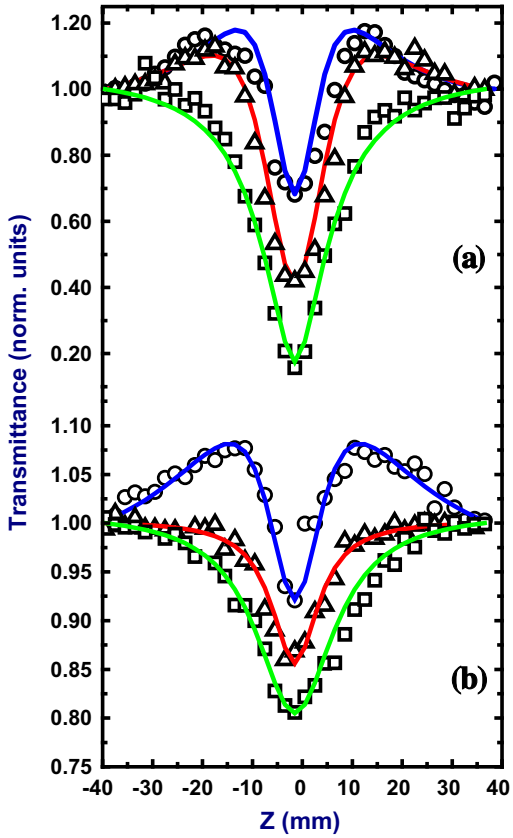

Figure 3. Open aperture Z-Scan curves obtained for (a) Colloidal-CCl_4 with varying input intensities I_{00} = 96 GW/cm^2 (open circles), I_{00} = 130 GW/cm^2 (open triangles) and I_{00} = 190 GW/cm^2 (open squares) (b) Colloidal-$CHCl_3$ with varying input intensities I_{00} = 69 GW/cm^2 (open circles), I_{00} = 110 GW/cm^2 (open triangles) and I_{00} = 140 GW/cm^2 (open squares). Solid lines are theoretical fits.

size and shape of the NPs. We feel that the coefficients presented in our study are better than some of the above mentioned and needs further exploration, especially the SPR enhancement in Al NP's.

4. Conclusions

In summary, FLA of bulk Al sample in oxygen free liquid media like CCl_4 and $CHCl_3$ in atmosphere led to Al nanoparticle generation with less oxide cladding and different nanostructure formation. The size of the generated nanoparticles depended not only upon laser parameters but also on the polarity of liquid environment. We could generate smaller nanoparticles in polar liquid ($CHCl_3$) compared to non-polar liquid (CCl_4). The average size of Al NPs was 20–40 nm in CCl_4 and 10–25 nm in $CHCl_3$. The nonlinear absorption behavior was complicated in both the cases.

Acknowledgements

This work is supported by DRDO, India.

References

[1] S. Eliezer, N. Eliaz, E. Grossman, Laser Part. Beams 23 (2005) 15.
[2] S. Link, M.A. El- Syed, Annu. Rev. Phys. Chem. 54 (2003) 331.
[3] S.L. Stoll, E.G. Gillan, A.R. Barron, Chem. Vap. Deposition 2 (1996) 182.
[4] S. Banerjee, S. Roy, J.W. Chen, D. Chakravorthy, J. Magn. Magn. Mater. 45 (2000) 219.
[5] W. Abdul-Razzaq, M.S. Seehra, Phys. Status Solidi A 94 (2002) 193.
[6] K. Sturm, S. Fahler, H.-U. Krebs, Appl. Surf. Sci. 462 (2000) 154.
[7] S. Eliezer, N. Eliaz, E. Grossman, Phys. Rev. B 69 (2004) 144119.
[8] G. A. Shafeev, Nova Science Publishers Inc., (2008) 1.
[9] E. Stratakis, V. Zorba, M. Barberoglou, C. Fotakis, G.A. Shafeev, Nanotechnology 20 (10) (2009) 10530.
[10] J. Radziemski, D.A. Creamers, Laser Induced Plasma and Applications, Marcel Dekker, New York, 1989.
[11] V.A. Karavanskii, A.V. Simakin, V.I. Krasovskii, P.V. Ivanchenko, Quantum Electron. 34 (2004) 644.
[12] R.M. Tilaki, A. Irajizad, S.M. Mahdavi, Appl. Phys A 84 (2006) 215.
[13] P.V. Kazakevich, A.V. Simakin, G.A. Shafeev, Quantum Electron. 35 (2005) 831.
[14] J. Suna, S.L. Simon, Thermochima Acta 463 (2007) 32.
[15] E. Stratakis, V. Zorba, M. Barberoglou, C. Fotakis, G.A. Shafeev, Appl. Surf. Sci. 255 (2009) 5346.
[16] E. Stratakis, M. Barberoglou, C. Fotakis, G. Viau, C. Garcia, G.A. Shafeev, Opt. Express 17 (2009) 12650.
[17] M. Sheik-Bahae, A.A. Said, E.W. Vanstryland, Opt. Lett. 14 (1989) 955.
[18] M. Yin, H.P. Li, S.H. Tang, W. Ji, Appl. Phys. B 70 (2000) 587.
[19] S. Venugopal Rao, T. Shuvan Prashant, T. Sarma, Pradeepta K. Panda, D. Swain, Surya P. Tewari, Chem. Phys. Lett. 514 (2011) 98.
[20] P.T. Anusha, P. Silviya Reeta, L. Giribabu, Surya P. Tewari, S. Venugopal Rao, Mater. Lett. 64 (2010) 1915.
[21] A. Baladi, R.S. Mamoory, Appl. Surf. Sci. 256 (2010) 7559.
[22] E.V. Zavedeev, A.V. Petrovskaya, A.V. Simakin, G.A. Shafeev, Quant. Electron. 36 (2006) 978.
[23] S. Lau Truong, G. Levi, F. Bozon-Verduraz, A.V. Petrovskaya, A.V. Simakin, G.A. Shafeev, Appl. Phys. A89 (2007) 373.
[24] A. Hamdorf, M. Olson, C.H. Lin, L. Jiang, J. Zhou, H. Xiao, H. L. Tsai1, Opt. Lett. 36 (2011) 3353.
[25] Y. Gao et al., Opt. Commun. 251 (2005) 429.
[26] M. Samoc, A. Samoc, B. Luther Davies, H. Reisch, U. Scherf, Opt. Lett. 23 (1998) 129.
[27] M. Sheik-Bahae, A.A. Said, T.H. Wei, D.J. Hagan, E.W. Van Stryland, IEEE J. Quant. Electron. 26 (1990) 760.
[28] B. Gu, W. Ji, Opt. Exp. 16 (2008) 10208.
[29] K. Venkata Saravanan, K.C. James Raju, M.G. Krishna, Surya P. Tewari, S. Venugopal Rao, Appl. Phys. Lett. 96 (2010) 232905.
[30] S. Wang, Y. Yang, H. Yu, D. Dlott, Prop. Explos. Pyrotech. 30 (2005) 148.
[31] S. Venugopal Rao, J. Mod. Opt. 58 (2011) 1024.
[32] Y.H. Lee, Y. Yan, P. Lakshminarayana, Q.H. Xua, Appl. Phys. Lett. 95 (2009) 023105.
[33] L. De Boni, E.L. Wood, C. Toro, F.E. Hernandez, Plasmonics 3 (2008) 171.
[34] R. Philip, G.R. Kumar, N. Sandhyarani, T. Pradeep, Phys. Rev. B62 (2000) 13160.
[35] H.I. Elim, J. Yang, J.Y. Lee, J. Mi, W. Ji, Appl. Phys. Lett. 88 (2006) 083107.
[36] R. Sathyavathi, M. Balamurali Krishna, S. Venugopal Rao, R. Saritha, D. Narayana Rao, Adv. Sci. Lett. 3 (2010) 138.